Article

Discovery Medicine 2026; 38(208): 1492–1506
https://doi.org/10.24976/Discov.Med.202638208.116

Meconium Microbiome–Metabolome Profiling at Birth Identifies Azelaic Acid as a Candidate Signal in Neonatal Hyperbilirubinemia

Zhongyuan Li[1], Yan Zhang[2], Qiuhong Wang[3], Lihua Peng[2], Xiaohong Hu[1], Liping Zou[4,*]

[1]Senior Department of Pediatrics, Chinese PLA General Hospital, 100010 Beijing, China
[2]Microbiota Laboratory, Clinical Division of Microbiota, Department of Gastroenterology and Hepatology, Chinese PLA General Hospital, 100853 Beijing, China
[3]Department of Neurology, Beijing Children's Hospital, Capital Medical University, 100045 Beijing, China
[4]Department of Pediatrics, The First Medical Center, Chinese PLA General Hospital, 100853 Beijing, China
*Correspondence: zouliping21@hotmail.com (Liping Zou)
Submitted: 3 February 2026 Revised: 26 March 2026 Accepted: 16 April 2026 Published: 20 May 2026

Background: Neonatal hyperbilirubinemia (HB) is common in the first postnatal week, and early gut ecological and metabolic features may influence bilirubin homeostasis via the gut–liver axis. We sought birth meconium microbiome–metabolome features linked to HB and evaluated a candidate metabolite *in vivo*.

Methods: First-pass meconium was collected within 24 h from 219 neonates. A nested case–control subset was analyzed (HB, n = 21; Healthy Controls (HC), n = 39). Microbiota were profiled by 16S rRNA gene sequencing (V3–V4), and metabolites were quantified using a targeted absolute-quantification LC–MS panel (Q300). Community structure was assessed using weighted and unweighted UniFrac distances and tested by analysis of similarities (ANOSIM), with PERMDISP used to evaluate dispersion. Genus-level differences were explored by LEfSe and interpreted cautiously given the low-biomass nature of meconium. Metabolites were compared by univariate testing, visualized by volcano plots, and adjusted using false discovery rate (FDR). Azelaic acid (AzA) was tested in an acetylphenylhydrazine-induced rat model with serum total bilirubin, colonic occludin, colonic β-glucuronidase activity, and fecal 16S profiling.

Results: HB and HC showed modest but statistically significant differences in weighted and unweighted UniFrac distances (weighted R = 0.1965, p = 0.0030; unweighted R = 0.1225, p = 0.0100). Metabolomics showed limited global separation; AzA was lower in HB on nominal testing, but no metabolite remained significant after FDR correction. In rats, AzA was associated with lower serum total bilirubin, directionally higher colonic occludin, decreased colonic β-glucuronidase activity, and suggested a partial shift in fecal community structure toward controls.

Conclusions: Birth meconium profiling nominated lower AzA as a hypothesis-generating signal; the rat experiment provides complementary, biologically plausible evidence. Replication in independent neonatal datasets is warranted.

Keywords: neonatal hyperbilirubinemia; gut microbiome; meconium; metabolomics; azelaic acid; intestinal barrier

Introduction

Neonatal hyperbilirubinemia (HB) remains one of the most common reasons for postnatal evaluation and hospital readmission among otherwise healthy term infants, and guideline-driven management continues to evolve as evidence accumulates regarding treatment thresholds and follow-up strategies [1]. Although most neonatal jaundice are transient and self-limited, clinically significant bilirubin elevation still carries a non-trivial risk of bilirubin-induced neurologic dysfunction when recognition or intervention is delayed [2,3]. Contemporary practice therefore seeks to balance prevention of neurotoxicity against avoidance of unnecessary intervention, particularly the overuse of phototherapy [1,4]. Despite increasingly refined clinical algorithms, the biological determinants that shift an infant from physiologic jaundice toward treatment-requiring HB remain incompletely defined, and actionable, mechanism-informed biomarkers available at birth are limited [2,3].

Bilirubin homeostasis in the early neonatal period is influenced not only by hepatic conjugation capacity but also by intestinal handling and enterohepatic cycling. Conjugated bilirubin delivered to the gut may undergo deconjugation and reabsorption, thereby augmenting systemic bilirubin exposure—an effect that is particularly relevant when enteral intake is limited and intestinal transit is delayed. A key microbial contributor to this process is β-glucuronidase activity, which can liberate unconjugated bilirubin from its glucuronides and facilitate reabsorption [5,6]. Beyond β-glucuronidases, recent studies have renewed interest in additional microbial bilirubin-transforming path-

ways. Bilirubin-reducing bacteria and enzymes have been described in the intestinal ecosystem, supporting the concept that microbial functional potential may influence luminal bilirubin fate [7,8]. In parallel, intestinal barrier integrity has been proposed as an additional modulator of enterohepatic cycling, through effects on mucosal permeability, inflammatory tone, and the luminal enzymatic environment, positioning epithelial tight junction biology as a plausible component of the gut–liver axis relevant to neonatal bilirubin kinetics [9,10].

These mechanisms intersect with a critical temporal window in early life, as initial microbial assembly begins immediately after birth and is strongly patterned by delivery mode, feeding practices, and perinatal exposures [11,12]. Meconium—despite being a low-biomass matrix that requires careful contamination-aware interpretation—offers a unique baseline specimen captured before most postnatal interventions and often prior to clinical outcome ascertainment. Accumulating evidence indicates that first-pass meconium can harbor a detectable microbial signal and may reflect early functional programming relevant to downstream host phenotypes [13,14]. However, most clinical studies examining links between the neonatal microbiome and jaundice have relied on stool collected after jaundice recognition and/or after initiation of phototherapy, complicating efforts to disentangle antecedent biological risk from treatment- or feeding-related effects [15–17]. Moreover, many reports remain primarily taxonomy-focused, without integrating the metabolite context through which microbes interface with bilirubin cycling and mucosal physiology.

Multi-omics approaches are increasingly being applied to address these limitations. Recent work combining microbial and metabolic profiling has implicated altered gut bacteria and bile acid metabolism as an axis associated with neonatal jaundice, highlighting the potential value of metabolite-centered readouts that may lie closer to mechanism than community composition alone [18]. Nevertheless, birth-proximal, outcome-agnostic sampling designs and metabolite-anchored candidates that can be experimentally interrogated remain scarce. This gap is notable because metabolites are, in principle, tractable: they can serve as biomarkers, mechanistic probes, and—if safety and biological plausibility permit—targets for functional validation.

Within this conceptual framework, azelaic acid (AzA), a naturally occurring dicarboxylic acid with established clinical use in dermatology, emerges as a biologically plausible candidate. Beyond its antimicrobial and anti-inflammatory properties, experimental studies in adult models have suggested that AzA can influence gut inflammation, barrier-associated readouts, and microbiota composition [19,20]. Although these contexts differ from neonatal HB, they support the broader notion that AzA can engage gut-centered pathways potentially relevant to enterohepatic bilirubin handling. Together with emerging recognition that microbial bilirubin metabolism is enzymatically programmable, these observations motivate investigation of an AzA-centered, gut-mediated hypothesis linking luminal enzymatic activity, barrier function, and bilirubin reabsorption.

We analyzed first-pass meconium collected at birth, prior to outcome ascertainment, and integrated 16S rRNA gene profiling with targeted absolute-quantification metabolomics within a nested case–control framework to identify early microbial and metabolic features associated with subsequent neonatal HB. On the basis of hypothesis-generating metabolite screening and biological plausibility, AzA was prioritized as a candidate for functional follow-up. We further explored the effects of AzA in an acetylphenylhydrazine-induced hyperbilirubinemia rat model, focusing on intestinal readouts relevant to bilirubin deconjugation and barrier-associated proteins, in accordance with contemporary expectations for transparent animal research reporting [21]. Given the exploratory nature of birth meconium profiling, candidate signals identified in this setting were interpreted cautiously and require independent validation.

Methods

Study Design, Setting, and Ethics

This study was conducted as a nested case–control analysis within a prospective birth cohort established at four tertiary maternity centers in Beijing, China (July 2022–January 2023), including the Fourth Medical Center of the Chinese PLA General Hospital, the Sixth Medical Center of the Chinese PLA General Hospital, the Air Force Specialty Medical Center, and the Aviation General Hospital. The cohort was conducted under an ongoing ethics approval granted by the Ethics Committee of the Seventh Medical Center, Chinese PLA General Hospital (Approval No.2021-033). Written informed consent was obtained from parents or legal guardians prior to participation. All procedures were conducted in accordance with the Declaration of Helsinki and relevant regulations.

Cases were defined as newborns diagnosed with neonatal HB based on age-specific total serum bilirubin (TSB) thresholds specified in the Chinese Medical Association Expert Consensus (2014) [22]. The control group comprised newborns whose bilirubin levels did not meet the diagnostic threshold for HB and were randomly selected from the same cohort. Controls were randomly sampled from eligible infants within the same birth cohort after applying the same inclusion and exclusion criteria, using a computer-generated random number list and without individual matching. To minimize interference from perinatal factors affecting early microbial exposure, both cases and controls were selected from the same cohort and restricted to full-term singleton vaginal deliveries. Case-control sampling followed a predefined protocol, prioritizing consis-

tency in key perinatal variables and sample collection timing. Clinical management of HB adhered to consensus guidelines, including phototherapy when indicated during routine clinical care.

Participant Eligibility and Clinical Data Collection

Neonates were eligible if their mothers were generally healthy, had routine prenatal care, and had no major comorbidities during pregnancy (including gestational diabetes, hypertension, or thyroid dysfunction). Additional eligibility criteria were maternal absence of systemic antibiotic exposure within 1 week prior to delivery, and term vaginal birth (gestational age $\geq$37 and $<$42 weeks) with birth weight 2500–$<$4000 g. Infants were required to have no birth asphyxia (Apgar scores $\geq$8 at 1, 5, and 10 min), and first-pass meconium had to be successfully collected within 24 h after birth. Parents/guardians provided written informed consent for meconium sampling and agreed to follow-up assessment at approximately 1 month of age to ascertain whether neonatal HB was diagnosed.

Infants were excluded if key perinatal data (birth weight, gestational age, or Apgar scores) were incomplete; if HB was attributable to identifiable secondary causes (e.g., hemolytic jaundice including ABO/Rh incompatibility, glucose-6-phosphate dehydrogenase deficiency, clinically significant cephalohematoma or other major hematoma, biliary obstruction, or breast milk jaundice); if the neonate was diagnosed with conditions other than HB during the neonatal period; if formula supplementation reached $\geq$3 feeds per day during the neonatal period; if the infant received antibiotics or probiotics during the neonatal period; if meconium collection failed; if follow-up could not confirm whether HB was diagnosed (including infants noted to have jaundice who did not present for clinical evaluation); or if parents/guardians withdrew consent for any reason.

A total of 219 neonates were enrolled in the cohort. The final nested case–control subset used for multi-omics analysis comprised 21 infants with HB and 39 healthy controls (HC). Demographic and perinatal variables (sex, gestational age, birth weight, feeding pattern during hospitalization, and perinatal antibiotic exposure, when applicable) were extracted from the electronic medical record and follow-up telephone interviews were conducted.

Meconium Collection, Handling, and Storage

Meconium samples were collected as the first-pass stool within 24 h after birth by trained nurses using standardized procedures. Sterile fecal collection tubes and disposable sterile swabs were used for all collections. To minimize environmental contamination, collection was performed prior to application of diaper creams, and contact with non-sterile surfaces was avoided. Immediately after passage, meconium was transferred into sterile containers, temporarily stored at –20 °C, and transferred within 24 h to –80 °C freezers. During downstream handling, single-use consumables and filtered pipette tips were used, and samples were processed in small batches under standardized conditions. All samples were subsequently transported on dry ice for downstream analyses.

Meconium DNA Extraction and 16S Sequencing

Microbial DNA was extracted from first-pass meconium using a magnetic bead–based extraction workflow with mechanical disruption (bead beating) following the sequencing service provider's validated protocol (Majorbio Bio-Pharm Technology Co., Ltd., Shanghai, China). DNA quantity and purity were assessed using a NanoDrop 2000 spectrophotometer (Thermo Fisher Scientific, Waltham, MA, USA), and integrity was checked by 1% agarose gel electrophoresis.

The V3–V4 region of the bacterial 16S rRNA gene was amplified using primers 338F (5′-ACTCCTACGGGAGGCAGCAG-3′) and 806R (5′-GGACTACHVGGGTWTCTAAT-3′). PCR was performed in triplicate using 20 μL reaction mixtures containing 4 μL of 5× FastPfu buffer, 2 μL of dNTP mix (2.5 mM each), 0.8 μL of each primer (5 μM), 0.4 μL of FastPfu DNA polymerase, 0.2 μL of bovine serum albumin, ~10 ng of template DNA, and nuclease-free water. Thermal cycling was 95 °C for 3 min; 30 cycles of 95 °C for 30 s, 55 °C for 30 s, and 72 °C for 45 s; followed by 72 °C for 10 min and holding at 10 °C. Triplicate amplicons were pooled per sample, verified on 2% agarose gels, purified by magnetic-bead cleanup, quantified, pooled equimolarly, and used for library construction with the NEXTFLEX Rapid DNA-Seq Kit. Libraries were sequenced on an Illumina MiSeq PE300 platform (2 × 300 bp) by Majorbio Bio-Pharm Technology Co., Ltd. (Shanghai, China).

16S Bioinformatics and Statistical Analyses

For the neonatal meconium V3–V4 dataset generated on the Illumina MiSeq PE300 platform (Illumina, San Diego, CA, USA), raw reads were quality filtered using fastp (v0.20.0), merged using FLASH (v1.2.11), and imported into QIIME2 (v2022.2.0) for denoising and amplicon sequence variant (ASV) inference using DADA2, with chimera removal performed using the consensus method. Taxonomy was assigned using a naïve Bayes classifier trained on the SILVA database (v138) for the corresponding region.

Alpha diversity (Shannon and Simpson) and beta diversity (weighted and unweighted UniFrac) were computed in QIIME2, and principal coordinates analysis (PCoA) was used for ordination. For diversity analyses, samples were rarefied to 26,000 reads per sample. Group differences in community structure were evaluated using analysis of similarities (ANOSIM) (999 permutations), and PERMDISP was used to check whether group differences could be attributed to unequal dispersion. Exploratory genus-level dif-

ferential abundance screening was performed using LEfSe with a Kruskal–Wallis $p < 0.05$ and a linear discriminant analysis (LDA) score threshold >3.0. Because meconium is a low-biomass specimen and extraction/PCR blank controls were not processed alongside samples in the present study, genus-level findings were interpreted as exploratory only.

Targeted Metabolomics With Absolute Quantification

Targeted metabolomics profiling of meconium was performed using a commercial Q300 metabolite panel designed for absolute quantification (Q300 metabolic chip; Human Metabolomics Institute, Inc., Shenzhen, China). Approximately 5 mg of meconium was extracted using a methanol-based solvent containing internal standards and processed according to the manufacturer's validated workflow, including derivatization steps for applicable metabolite classes (e.g., organic acids), prior to LC–MS/MS analysis.

Chromatographic separation and mass spectrometric acquisition were conducted using the vendor's prevalidated Q300 quantitative method on an ultra-high-performance liquid chromatography–tandem mass spectrometry platform. Analyses were performed in both positive and negative electrospray ionization modes, and absolute concentrations were determined using internal standards and external calibration as specified by the Q300 workflow. Concentration tables were exported for downstream statistical analysis.

Exploratory Cross-Domain Analyses

Limited cross-domain analyses were prespecified as exploratory. Spearman correlation was used to relate absolute concentrations of selected metabolite candidates to PCoA coordinates derived from weighted UniFrac distances of the neonatal meconium V3–V4 (Illumina MiSeq PE300) dataset (**Supplementary Table 1**).

Animal Experiments and Intestinal Microenvironmental Readouts

An acetylphenylhydrazine (APH)-induced hyperbilirubinemia model was established in specific-pathogen-free male Sprague–Dawley rats obtained from SPF (Beijing) Biotechnology Co., Ltd. Rats were 6 weeks old and weighed 180–200 g at study entry. A total of 40 rats were used in this study and randomly assigned to four groups (n = 10/group): Ctrl, Model, LowDose, and HighDose. Rats were housed under controlled temperature and humidity with a 12 h light/dark cycle and provided standard chow and water ad libitum. HB was induced by intraperitoneal injection of freshly prepared 2% APH (Aladdin, Shanghai, China; Cat. No. A100226) at 1 mL/100 g on day 1 and 0.5 mL/100 g on day 3. Successful model establishment was defined as a significant elevation in serum total bilirubin in the APH-treated Model group relative to the Ctrl group at the prespecified endpoint. The Ctrl group received saline only, the Model group received APH induction followed by normal saline, and the LowDose and HighDose groups received APH induction followed by AzA (Aladdin, Shanghai, China; Cat. No. A108439) gavage at 12 mg/100 g/day and 24 mg/100 g/day, respectively. Outcome assessment was performed in a blinded manner. From day 4 to day 8, AzA was administered by oral gavage once daily at 12 mg/100 g/day or 24 mg/100 g/day; control groups received an equivalent volume of normal saline. Animals were monitored daily throughout the experimental period. The overall experimental timeline is shown in **Supplementary Fig. 1**.

At 17:00 on day 8, rats were single-housed without bedding, with sterile filter paper placed in the cage. Fecal pellets were collected from each rat into sterile 15 mL tubes prior to necropsy, stored temporarily at –20 °C, and transferred on dry ice within 24 h to –80 °C for long-term storage until microbiome sequencing. On the morning of day 9, rats were deeply anesthetized with inhaled isoflurane (3%–5% for induction; EZVET, Beijing Yizejia Technology Co., Ltd.; batch no. G45993) followed by euthanasia via cervical dislocation. Blood was collected from the abdominal aorta for serum total bilirubin measurement. The colon (from the distal cecum to the proximal rectum) was harvested for assessment of luminal pH (via colonic lavage), colonic β-glucuronidase activity, and tight-junction protein expression (occludin and ZO-1).

Serum total bilirubin was measured using a commercial kit (Solarbio, Beijing, China; Cat. No. BC5185) according to the manufacturer's instructions, with absorbance read on a SpectraMax M5 microplate reader (Molecular Devices, San Jose, CA, USA).

For luminal pH assessment, the colonic lumen was flushed with 1 mL sterile normal saline, and the lavage fluid was measured immediately using pH indicator strips (Merck, Darmstadt, Germany; Cat. Nos. 1.09542.0001 and 1.09543.0001) according to the manufacturer's instructions.

Colonic β-glucuronidase activity was measured using a commercial enzymatic assay kit (Enzyme-linked Biotechnology Co., Ltd., Shanghai, China; Cat. No. ml076743) according to the manufacturer's instructions. Briefly, colonic samples were homogenized in assay buffer, clarified by centrifugation, and incubated with substrates in a 96-well plate at 37 °C for 30 min. Absorbance was read at 540 nm on a SpectraMax M5 microplate reader (Molecular Devices, San Jose, CA, USA), and enzyme activity was normalized to total protein concentration determined by BCA assay and expressed as μmol/h/mg protein.

For western blot analysis, colonic tissues were homogenized in ice-cold RIPA lysis buffer (Solarbio; Cat. No. R0010) supplemented with protease inhibitor (Solarbio; Cat. No. P6730), and protein concentration was determined using a BCA kit (Solarbio; Cat. No. PC0020).

Equal amounts of protein were separated by SDS–PAGE and transferred onto 0.22 µm nitrocellulose membranes by wet transfer at 100 V for 1 h. After washing with 1×TBST, membranes were blocked for 1 h at room temperature and incubated overnight at 4 °C with primary antibodies against β-actin (Affinity, Cat. No. T0022; 1:1000), occludin (Proteintech, Cat. No. 27260-1-AP; 1:5000), and ZO-1 (Proteintech, Cat. No. 21773-1-AP; 1:5000). Membranes were then washed three times in TBST (10 min each) and incubated for 1 h at room temperature with HRP-conjugated secondary antibodies (Cellway Lab, Cat. Nos. C030270 and C030272; 1:5000) diluted in 3% non-fat milk in 1× TBST. Protein bands were visualized using enhanced chemiluminescence and imaged on a ChemiScope 6100 system (CLINX, Shanghai, China). Band intensity was quantified by densitometry using ImageJ (version 1.53, National Institutes of Health, Bethesda, MD, USA). β-actin was used as the loading control.

All animal procedures were approved by the Experimental Animal Ethics Committee of Kangtai Medical Laboratory Service Hebei Co., Ltd. (Approval No. MDL2025-06-03-02).

Rat Fecal Full-Length 16S rRNA Gene Sequencing

Rat fecal microbiome profiling was performed using third-generation, full-length 16S rRNA gene sequencing. Microbial DNA was extracted from fecal pellets using the TIANMicrobe Magnetic Envir-DNA Kit 4 (TIANGEN Biotech; Cat. No. DP713-T8). The full-length 16S rRNA gene was amplified using primers 27F (AGRGTTYGATYMTGGCTCAG) and 1492R (RGYTACCTTGTTACGACTT) in triplicate 20 µL reactions. PCR cycling was 95 °C for 3 min; 27 cycles of 95 °C for 30 s, 60 °C for 30 s, and 72 °C for 45 s; followed by 72 °C for 10 min and then held at 10 °C. Triplicate amplicons were pooled per sample and verified on 2% agarose gels. Amplicons were purified using a commercial gel-based cleanup workflow with magnetic-bead capture, then quantified and pooled according to the required sequencing depth.

SMRTbell libraries were constructed using the SMRTbell prep kit 3.0 and sequenced on a PacBio Sequel IIe System (Majorbio Bio-Pharm Technology Co., Ltd., Shanghai, China). Raw reads were processed using SMRT Link (v11.0) to generate HiFi reads (minimum full passes = 3; minimum predicted accuracy = 0.99), demultiplexed by barcodes, and length-filtered to retain bacterial 16S reads (1000–1800 bp). Downstream ASV inference and taxonomy assignment were performed in a QIIME2-based workflow consistent with the study's microbiome analyses (DADA2; SILVA v138). Diversity analyses were conducted after normalizing sequencing depth by rarefaction to a uniform depth across retained samples.

Statistical Analysis

Continuous variables were summarized as mean ± standard deviation or median (interquartile range), and categorical variables as counts (percentages). Normality of continuous variables was assessed using the Shapiro–Wilk test. Between-group comparisons used the independent-samples t test or the Mann–Whitney U/Wilcoxon rank-sum test for continuous variables and Pearson's χ^2 test or Fisher's exact test for categorical variables, as appropriate. For microbiome data, alpha-diversity comparisons used non-parametric tests when distributional assumptions were not met. Community-level differences were evaluated using ANOSIM on UniFrac distance matrices, with homogeneity of multivariate dispersion assessed using PERMDISP prior to interpretation.

For targeted metabolomics, absolute concentrations derived from kit calibration curves were compared between groups using parametric or non-parametric tests depending on distribution. For multi-group comparisons in the animal study, one-way ANOVA or the Kruskal–Wallis test was used as appropriate. When one-way ANOVA was used, post hoc pairwise comparisons were performed using Tukey's HSD test. When the Kruskal–Wallis test was used, post hoc pairwise comparisons were performed using Dunn's test with Holm adjustment. Multiple testing control for targeted metabolomics and selected post hoc analyses was performed using the Benjamini–Hochberg false discovery rate (FDR), with $q < 0.05$ considered statistically significant where applicable. Correlation analyses and lightweight cross-domain linkage analyses were predefined as exploratory. Statistical analyses were performed in R (v4.2.0) and GraphPad Prism (v9.0.0; GraphPad Software, San Diego, CA, USA). A two-sided p value < 0.05 was considered statistically significant unless otherwise specified, with exploratory analyses interpreted descriptively.

Results

Study Population and Overall Design

A total of 219 neonates were included in the prospective birth cohort. First-pass meconium was collected within 24 h of birth using sterile procedures and subsequently processed and stored at –80 °C. All infants were followed throughout the neonatal period to ascertain the occurrence of HB according to established clinical criteria. Using a nested case–control design, meconium samples from infants who developed HB and from infants who were never diagnosed with HB were selected for downstream analyses. Of the initially selected samples, 21 neonates with HB and 42 HC were included. Following microbiome and metabolomics quality control, three control samples were excluded due to insufficient sample quality, resulting in a final analytic set of 21 HB and 39 HC samples. The overall study workflow, including cohort inclusion, follow-up,

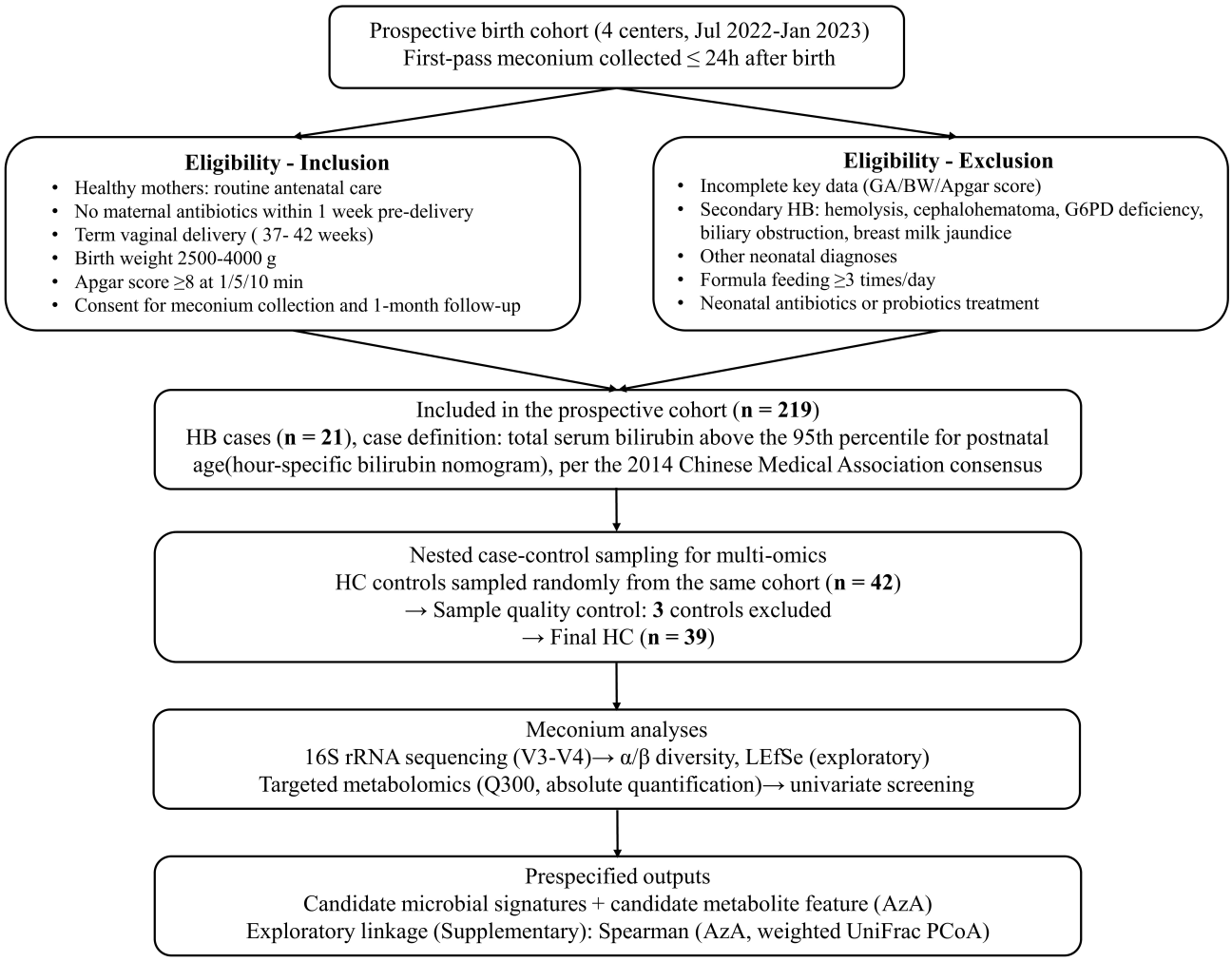

Fig. 1. Workflow of the neonatal research and nested case-control design. A prospective birth cohort was established between July 2022 and January 2023. Eligible mother–infant dyads were enrolled at delivery, and first-pass meconium was collected within 24 h after birth using standardized aseptic procedures. Neonatal hyperbilirubinemia (HB) was defined as total serum bilirubin exceeding age-specific thresholds according to the 2014 Chinese Medical Association consensus. Within the cohort, a nested case–control set was constructed, and meconium samples were selected for 16S rRNA gene sequencing (V3–V4) and targeted metabolomics using an absolute-quantification Q300 panel.

participant exclusions, and final analytic subsets, is summarized in Fig. 1.

The baseline maternal and neonatal characteristics of the study participants are summarized in Table 1. There were no statistically significant differences between the HB and HC groups with respect to maternal age, gestational age, pre-pregnancy weight, gestational weight gain, body mass index (BMI) before pregnancy or before delivery, neonatal birth weight, or infant sex distribution (all $p >$ 0.05).

All cases of HB were identified within the first postnatal week. Infants diagnosed with HB received standard phototherapy as part of routine clinical care, and serum total bilirubin levels declined during treatment. No bilirubin-related complications were observed during hospitalization.

Microbial Diversity and Community Structure in Meconium

Within-sample diversity was first compared between infants who developed HB and HC. Neither Shannon nor Simpson diversity indices differed between groups (Wilcoxon rank-sum test; Shannon, $p = 0.7038$; Simpson, $p = 0.8829$; Fig. 2A,B), indicating comparable overall meconium alpha diversity in this cohort.

Between-sample community structure was examined using UniFrac-based beta diversity. In principal coordinates analysis (PCoA), weighted and unweighted UniFrac distances showed partially overlapping distributions with a small shift in group centroids (Fig. 2C,D), alongside substantial inter-individual variability. Group differences in community composition were assessed using ANOSIM based on UniFrac distance matrices (weighted UniFrac, R

Table 1. Baseline characteristics of the study participants.

Variables	HB (n = 21)	HC (n = 39)	Statistical measure	*p*
Age (years)	32.00 (29.00–36.00)	31.00 (30.00–34.00)	Z = 0.46	0.651
Gestation period (days)	277.29 ± 7.23	276.69 ± 8.46	$t = 0.27$	0.786
Pre-pregnancy weight (kg)	57.26 ± 5.71	58.01 ± 6.33	$t = –0.45$	0.652
Weight before delivery (kg)	68.45 ± 6.32	69.10 ± 7.24	$t = –0.35$	0.731
Weight gain during gestation (kg)	11.19 ± 3.58	11.10 ± 4.10	$t = 0.08$	0.933
Pre-pregnancy BMI (kg/m^2)	22.08 ± 2.33	22.41 ± 2.44	$t = –0.52$	0.606
BMI before delivery (kg/m^2)	26.09 ± 2.65	26.39 ± 2.86	$t = –0.39$	0.697
BMI gain during gestation (kg/m^2)	4.01 ± 1.53	3.99 ± 1.64	$t = 0.05$	0.960
Birth weight (g)	3355.00 ± 357.20	3324.49 ± 323.24	$t = 0.34$	0.738
Sex (male/female)	14/7	16/23	$\chi^2 = 3.59$	0.058

Baseline maternal and neonatal variables are shown for descriptive comparison between the HB and HC groups. Age was compared using the Mann–Whitney U test and is reported with the corresponding standardized Z value. Categorical variables were compared using Pearson's χ^2 test, as all expected cell counts were $\geq$5. *p* values were not adjusted for multiple testing. HB, hyperbilirubinemia; HC, healthy control; BMI, body mass index.

= 0.1965, $p = 0.0030$; unweighted UniFrac, R = 0.1225, $p = 0.0100$). Multivariate dispersion was further evaluated using PERMDISP, which did not indicate differences in within-group dispersion between HB and HC (**Supplementary Table 2**). These results are consistent with a modest group-level shift in overall community structure, while emphasizing that the separation is modest and occurs against considerable between-infant variability.

Overall, these findings support a modest shift in meconium microbial community structure in relation to hyperbilirubinemia status, rather than a strongly discriminative separation between groups. The ANOSIM effect sizes were limited and should be interpreted in the context of substantial inter-individual variability and the relatively small sample size.

Differential Microbial Features Identified by LEfSe Analysis

Given the low-biomass nature of meconium and the absence of concurrent negative controls, genus-level findings are presented strictly as exploratory patterns rather than as evidence of colonizing taxa. To explore the genus-level features that may underlie the community-level shifts observed in beta diversity, LEfSe analysis was performed. A set of genera showing differential relative abundance between infants with HB and HC was identified and summarized by their linear discriminant analysis (LDA) effect sizes (Fig. 3). Fig. 3 presents the top 10 genera enriched in HB ranked by LDA score, together with all genera enriched in HC under the same LEfSe parameters. The complete list of detected features and associated statistics is provided in **Supplementary Table 3**.

The LEfSe-identified genera are therefore interpreted as hypothesis-generating signals only, and no mechanistic attribution to individual taxa is made in the present study.

Targeted Metabolomic Profiling of Meconium Samples

Targeted metabolomic profiling with absolute quantification (Q300 panel) was conducted in the meconium samples of infants with HB and HC to characterize early-life metabolic features. Across the 202 quantified metabolites, unsupervised principal component analysis (PCA) showed substantial overlap between groups, with no evident global separation in low-dimensional space (Fig. 4A). Consistent with this pattern, group comparisons of PC1 and PC2 scores were not significant (PC1, $p = 0.735$; PC2, $p = 0.559$), indicating that between-group differences were not captured as a dominant source of variance. At the individual-metabolite level, volcano plot screening identified a small number of features that were nominally significant, but none remained significant after false discovery rate correction (Fig. 4B; **Supplementary Tables 4,5**). Among these candidates, AzA was lower in HB than HC on nominal testing ($p = 0.0049$; Fig. 4C), although its FDR-adjusted q value did not support confirmatory inference.

Overall, the targeted absolute-quantification data suggest limited global metabolic separation between groups, with a small number of hypothesis-generating candidate features highlighted by univariate screening. These findings are interpreted as exploratory and warrant validation in independent cohorts.

Effects of AzA on HB, β-Glucuronidase Activity, and Barrier-Associated Proteins in an Animal Model

In the APH-induced rat model, serum total bilirubin levels were higher in the Model group than in controls at the prespecified endpoint (Fig. 5A). Administration of AzA was associated with a reduction in serum total bilirubin, with a larger reduction observed in the high-dose group (Fig. 5A).

Given the relevance of microbial deconjugation to enterohepatic bilirubin cycling, colonic β-glucuronidase

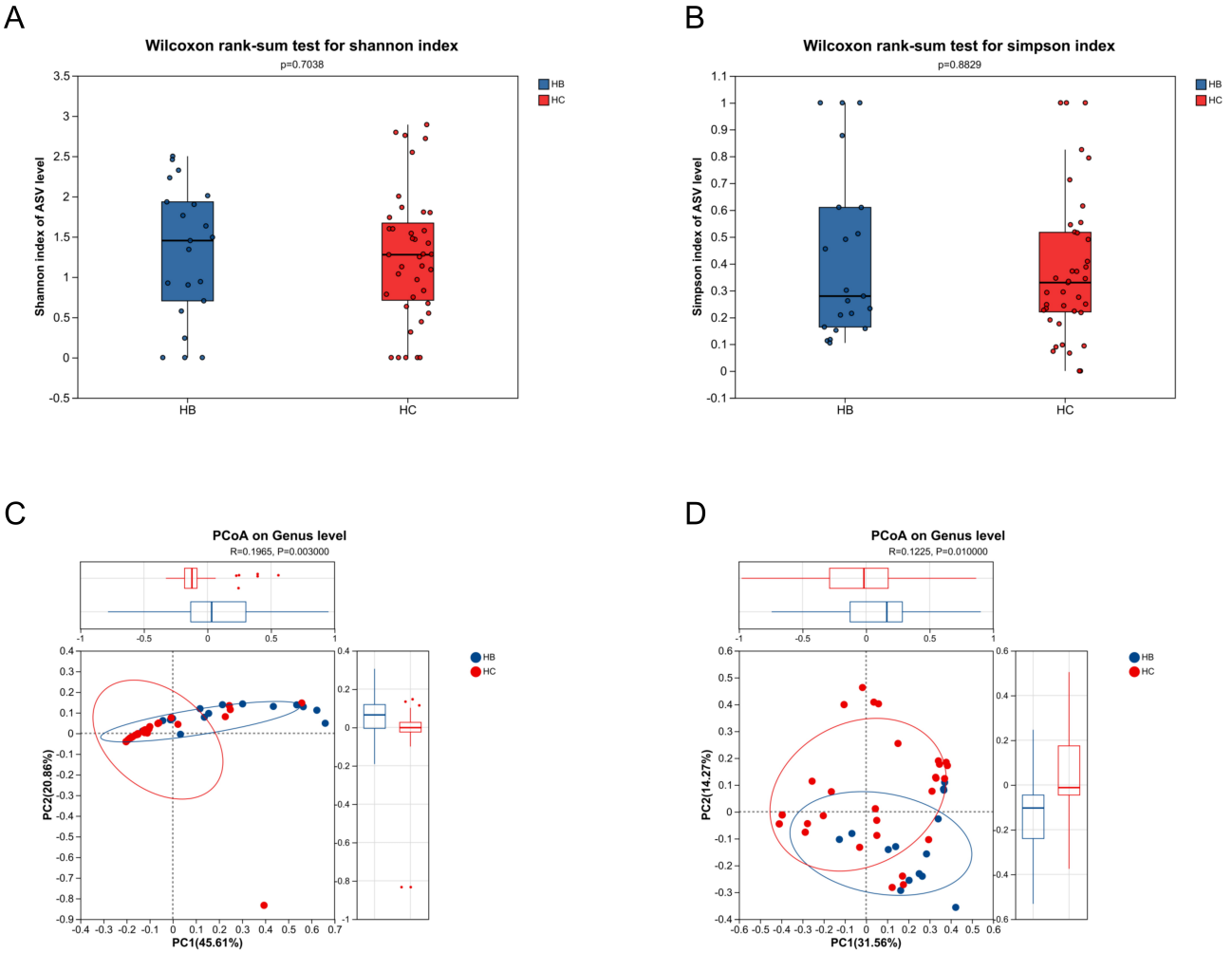

Fig. 2. Meconium microbial diversity and overall community structure in HB and healthy controls (HC). (A) Shannon diversity index of meconium microbiota; group comparison by Wilcoxon rank-sum test (p = 0.7038). (B) Simpson diversity index; group comparison by Wilcoxon rank-sum test (p = 0.8829). (C) Principal coordinates analysis (PCoA) based on weighted UniFrac distances (PC1 explains 45.61% of variation); group-level differences assessed by ANOSIM (R = 0.1965, p = 0.0030). (D) PCoA based on unweighted UniFrac distances (PC1 explains 31.56% of variation); group-level differences assessed by ANOSIM (R = 0.1225, p = 0.0100). Box-and-whisker plots show median (center line), interquartile range (box), and 1.5× IQR (whiskers), with individual samples overlaid as points. Each point in PCoA plots represents one infant; ellipses denote 95% confidence regions. Sample sizes: HB, n = 21; HC, n = 39. PC1, principal coordinate 1; ANOSIM, analysis of similarities; IQR, interquartile range.

activity was next examined. Compared with controls, β-glucuronidase activity was elevated in the Model group, whereas AzA-treated groups showed lower β-glucuronidase activity, with the lowest levels observed in the high-dose group (Fig. 5B).

For barrier-associated proteins, representative immunoblots are shown in Fig. 5C, and densitometric quantification is shown in Fig. 5D. Occludin expression was lower in the Model group and showed a directionally higher level following AzA administration. Given the small western blot sample size (n = 3/group) and the limited statistical annotations shown in Fig. 5D, these protein results should be interpreted cautiously. ZO-1 showed a similar directional pattern, with higher expression in the AzA-treated groups than in the Model group, but no statistically significant pairwise differences were observed under the present experimental conditions.

Finally, fecal 16S profiling suggested a partial shift in overall gut microbial community structure in AzA-treated animals toward that of the control group (**Supplementary Figs. 2,3**). No mortality or overt adverse effects were observed in any experimental group during the study period.

Discussion

Neonatal HB remains among the most frequent clinical problems in the early postnatal period, and a meaningful subset of infants reaches bilirubin levels that prompt treat-

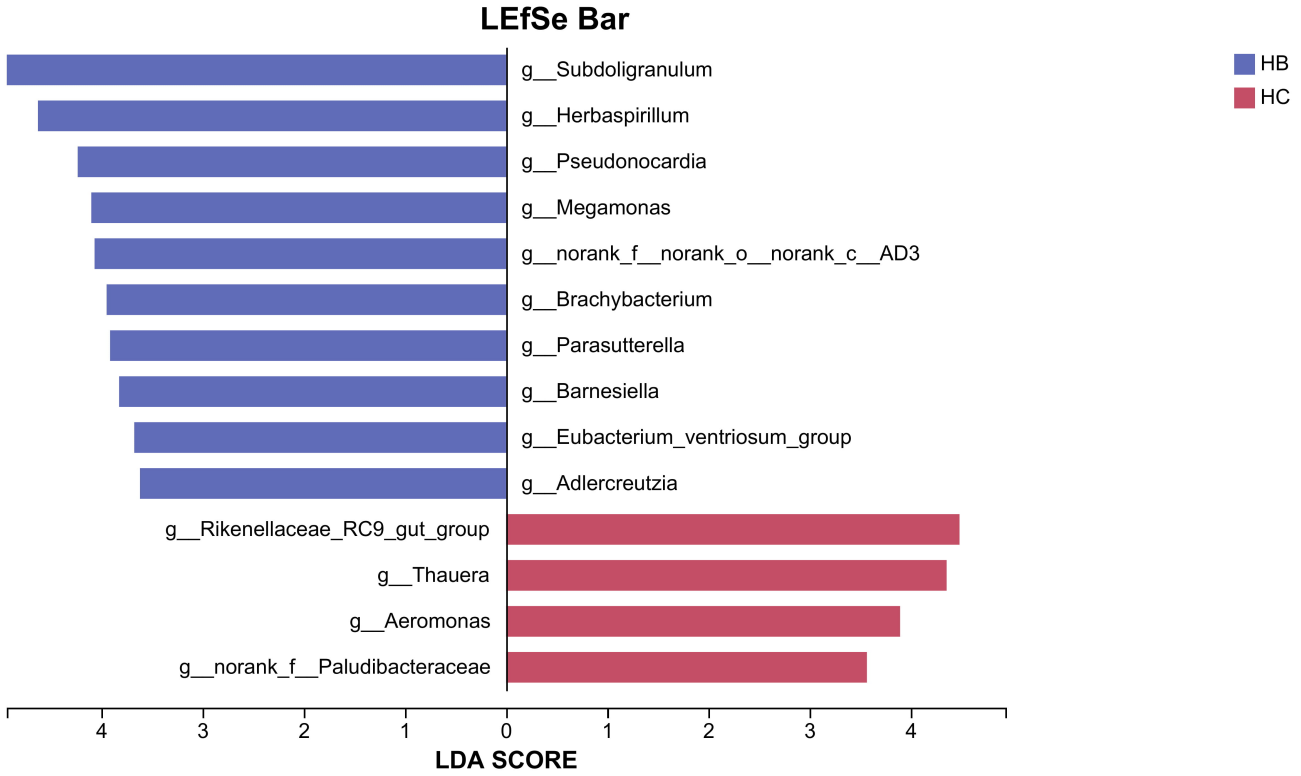

Fig. 3. Differential meconium microbial features identified by LEfSe at the genus level. LEfSe results are summarized by LDA effect size scores. Genera enriched in infants with hyperbilirubinemia (HB) are shown on the left and those enriched in healthy controls (HC) on the right. For clarity, the plot displays the top 10 HB-enriched genera ranked by LDA score, together with all HC-enriched genera identified under the same analysis settings. LEfSe parameters, including the significance threshold and LDA cutoff, are described in Methods. The complete LEfSe output and statistics are provided in **Supplementary Table 3**. Sample sizes: HB, n = 21; HC, n = 39. LEfSe, linear discriminant analysis effect size; LDA, linear discriminant analysis.

ment to reduce the risk of bilirubin neurotoxicity [23,24]. The canonical description of bilirubin handling has long been liver-centered, yet bilirubin enterohepatic circulation occurs in parallel with rapid, highly dynamic ecological succession in the neonatal gut during the first days of life, making the gut–liver axis a plausible additional layer of regulation [25,26]. We asked whether first-pass meconium collected at birth differs between infants who later develop HB and those who do not, and whether a candidate metabolite from these data can be tested experimentally. The results highlight three aligned observations: (i) community-level microbiome structure differed modestly between groups on weighted and unweighted UniFrac, (ii) targeted metabolomics identified nominal between-group differences—most notably AzA, which was lower in HB than HC on nominal testing, and (iii) in an acetylphenylhydrazine (APH)-induced HB rat model, AzA administration was associated with lower serum total bilirubin and barrier-related intestinal readouts. Two constraints are important: meconium is low biomass and vulnerable to background contamination, and metabolomics signals did not remain significant after FDR correction.

The microbiome findings are best interpreted at the community level. In the nested case–control analysis, both weighted and unweighted UniFrac indicated separation between HB and HC, implying that differences are not restricted to a single rare taxon but reflect broader compositional structure. This pattern is broadly consistent with an expanding literature linking neonatal jaundice to gut microbial shifts, including reports describing altered gut microbiota in infants with HB and changes following phototherapy [27,28], as well as recent synthesis work proposing microbiota-centered frameworks for jaundice development and heterogeneity [29]. What our data add, specifically, is that a signal is detectable as early as birth in meconium, before many of the postnatal exposures that rapidly remodel the gut community. However, the same timing that makes the question clinically appealing also makes interpretation fragile: in very early life, microbial biomass is extremely low, and apparent “differences” can reflect delivery-room transfer, early handling, or technical carryover as readily as biological colonization. Given this constraint, we use LEfSe to prioritize genera for follow-up rather than to define disease-associated taxa. Several taxa are biologically plausible in gut contexts, but some are also taxa that fre-

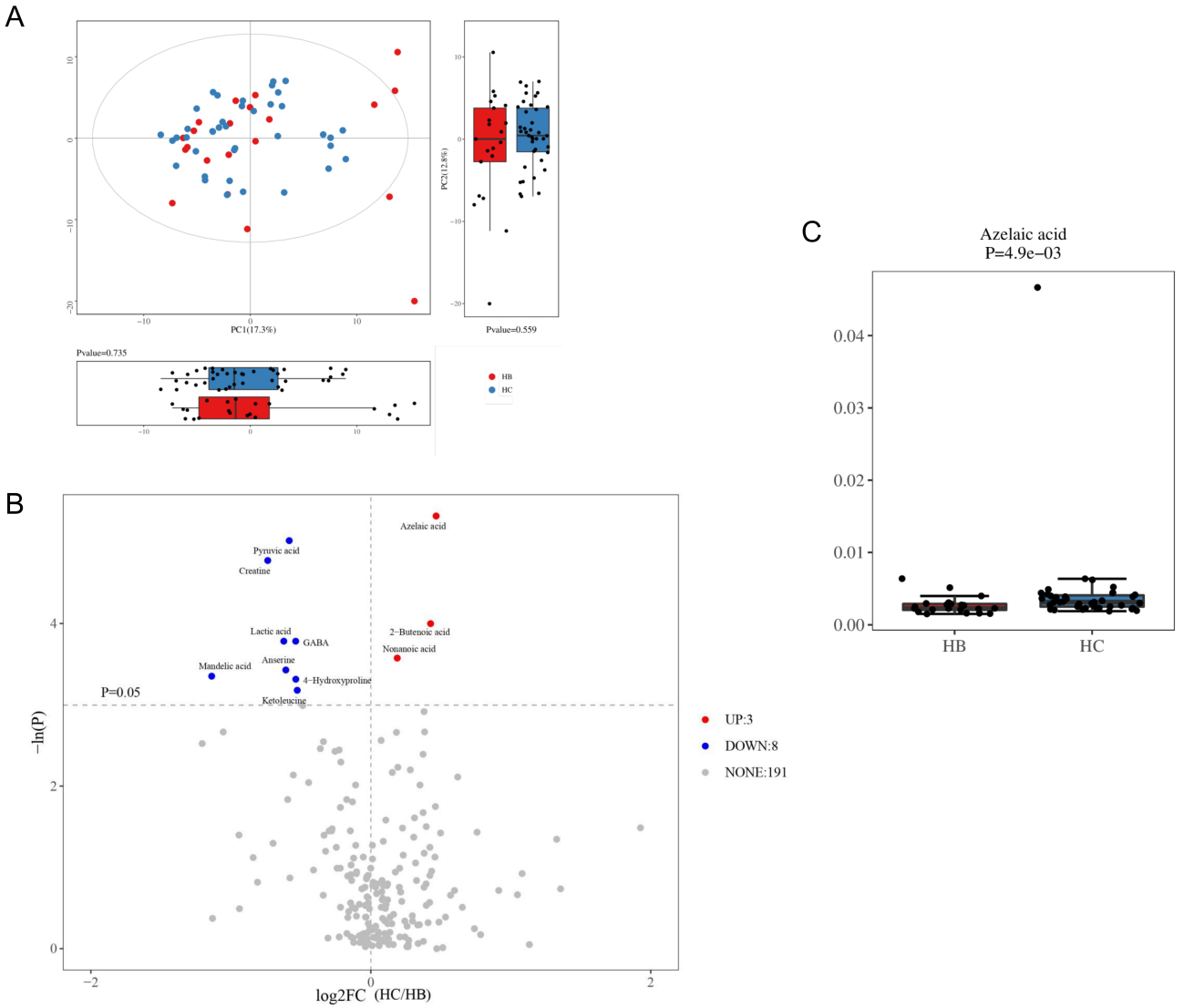

Fig. 4. Targeted metabolomics profiling of meconium using absolute quantification (Q300 panel). (A) PCA score plot based on absolute concentrations of the quantified metabolites. Insets show group-wise comparisons of PC1 and PC2 scores (*p*-values as indicated). (B) Volcano plot summarizing univariate comparisons between groups across the 202 quantified metabolites. The x-axis shows log2 fold change (HC vs HB), and the y-axis shows –log10(*p*). The dashed horizontal line indicates the nominal significance threshold ($p = 0.05$). Colored points indicate metabolites reaching nominal significance ($p < 0.05$), with red indicating higher and blue indicating lower concentrations in HC relative to HB. (C) Absolute concentration of AzA in HB and HC meconium (box-and-whisker plot; center line, median; box, interquartile range; whiskers, 1.5× IQR; points, individual infants); *p*-value as shown. The list of nominal candidate metabolites is provided in **Supplementary Table 4**, and the complete targeted metabolomics results, including FDR-adjusted *q*-values, are provided in **Supplementary Table 5**. HB, hyperbilirubinemia; HC, healthy controls; PCA, principal component analysis; AzA, azelaic acid. Sample sizes: HB, n = 21; HC, n = 39.

quently appear in low-biomass datasets and can be sensitive to laboratory background; that duality is precisely why genus-level claims in meconium demand caution.

Low-biomass microbiome work requires an explicit contamination framework, and this is a primary interpretive limitation for the present study. Multiple lines of evidence argue that very early meconium may not contain a stable indigenous microbiota, and that signals can be dominated by reagent and environmental contaminants once stringent negative controls are included [30,31]. Consensus guidance further emphasizes that cross-contamination and background signal can disproportionately influence low-biomass studies, and that transparent reporting and contaminant-control workflows should be treated as minimal standards rather than optional best practices [32]. In practice, without extraction blanks and PCR blanks processed alongside samples, one cannot confidently distinguish true low-abundance taxa from background signatures,

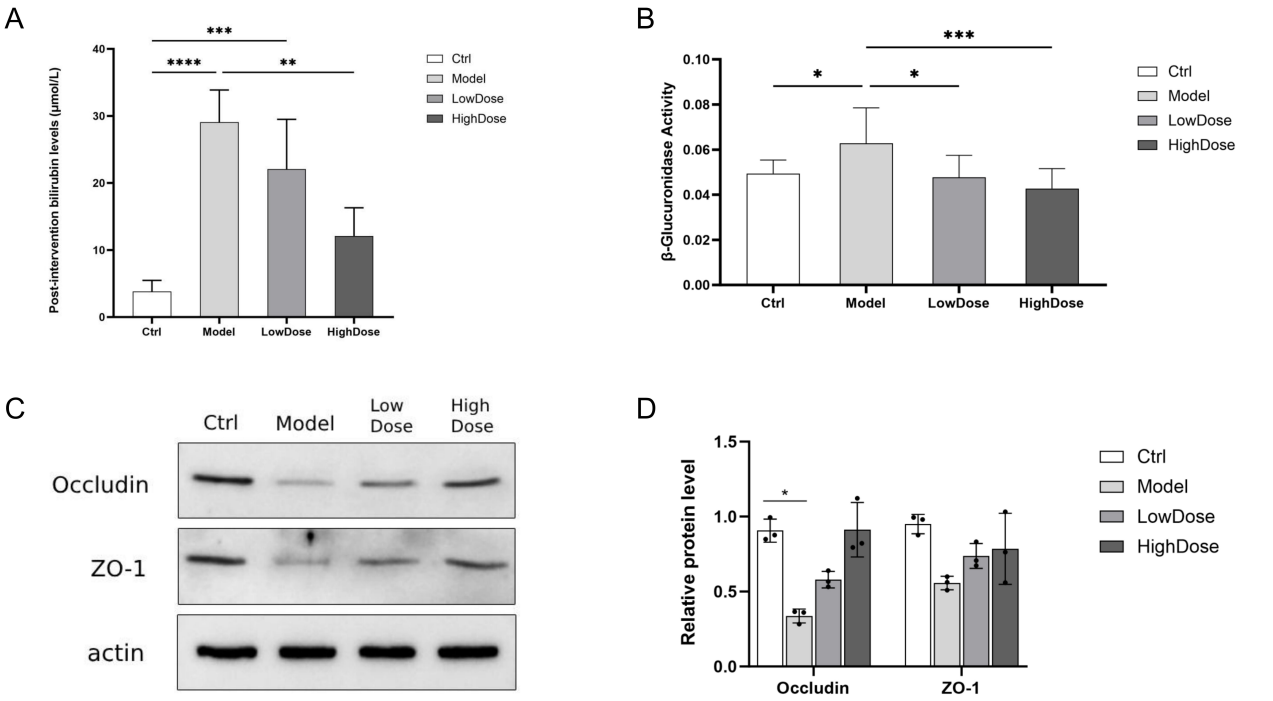

Fig. 5. Effects of azelaic acid (AzA) on an acetylphenylhydrazine-induced hyperbilirubinemia (HB) rat model. (A) Serum total bilirubin levels at the prespecified post-intervention endpoint in Ctrl, Model, LowDose, and HighDose groups. (B) Colonic β-glucuronidase activity measured as an enzymatic readout relevant to deconjugation processes. (C) Representative immunoblots of occludin and ZO-1 in colonic tissue. β-actin was detected on parallel membranes using the same protein samples to confirm loading consistency. (D) Densitometric analysis of occludin and ZO-1 expression relative to the corresponding β-actin measurements obtained from parallel membranes. Bars represent group summaries and points indicate individual animals. Statistical testing and multiple-comparison procedures were performed as described in the Methods section. Only statistically significant pairwise comparisons are annotated in the figure; non-significant comparisons are not shown. No statistically significant pairwise differences were observed for ZO-1. Significance levels are denoted in the figure (* $p < 0.05$, ** $p < 0.01$, *** $p < 0.001$, **** $p < 0.0001$). Ctrl, untreated control; Model, HB model; LowDose/HighDose, AzA treatment groups (doses as specified in Methods). ZO-1, zonula occludens-1. Sample sizes: n = 10/group for (A,B); n = 3/group for (C,D).

even when statistical separation is observed. This limitation constrains genus-level inference even when β-diversity separation is observed. In the present dataset, we therefore interpret the LEfSe-flagged genera as candidate signals that could arise from early exposure/transfer at delivery, immediate postnatal handling, and/or technical and processing effects that are amplified when biomass is low [33,34]. Future iterations should incorporate multiple negative controls (extraction blanks and PCR blanks), quantify bacterial load (e.g., qPCR-based 16S copy number), and apply formal decontamination pipelines using frequency- and prevalence-based contaminant identification [35]. Those steps would allow the same question to be revisited with a stronger basis for biological inference; until then, genus-level findings should remain explicitly exploratory.

A second, distinct methodological issue concerns the compositional nature of 16S rRNA gene data. Because our analysis relied on relative abundances, apparent between-group differences may partly reflect compositional shifts rather than absolute changes in microbial biomass [36]. Community-level β-diversity can still capture meaningful structure under compositional constraints, but genus-level differential abundance is particularly sensitive to both the statistical method selected and the presence of covariates. It is well documented that different differential abundance methods can yield inconsistent results across datasets, especially in sparse, low-biomass contexts [37]. LEfSe remains widely used, but it is not designed as a covariate-adjusted, bias-corrected confirmatory framework, and experts increasingly expect sensitivity analyses using methods that explicitly address compositional bias and allow covariate adjustment. ANCOM-BC2 is one modern option that provides a bias-corrected framework and can incorporate covariates in multi-group settings [38]. We did not apply ANCOM-BC2 or other multivariable association models here; accordingly, the most defensible microbiome claim in the present manuscript is limited to community-level differences with a set of exploratory candidate taxa, rather than mechanistic interpretations tied to specific genera.

The metabolomics results warrant a parallel level of restraint, but the logic differs from that used for high-dimensional untargeted discovery. Here, meconium metabolomics used a targeted, absolute-quantification LC–MS panel (Q300), meaning that metabolites were quantified against calibration standards and reported as absolute concentrations. In multivariate space, PCA did not show robust group separation, and at the metabolite level, multiple features showed nominal differences but none remained significant after FDR correction. That pattern can be read in two non-exclusive ways: the true effects may be modest with substantial inter-individual variability, and the available sample size (n) may be insufficient for multiple-testing-adjusted significance even when directionality is reproducible. The advantage of absolute quantification is that it increases confidence in the direction and magnitude of measured differences—useful for prioritization and follow-up—yet it does not solve the statistical power problem created by modest n and multiple comparisons. For that reason, we interpret the metabolite-level findings as hypothesis-generating signals measured by an absolute-quantification workflow, but statistically underpowered after multiple-testing correction [39,40].

Within that framework, AzA was selected as a pragmatic candidate for experimental evaluation. In the human meconium data, AzA was lower in HB than HC on nominal testing, but it did not meet significance after FDR correction; it therefore cannot be presented as a validated biomarker. The decision to prioritize AzA was based on tractability and biological plausibility rather than on statistical "winners". AzA has been reported to modulate inflammatory pathways and ameliorate colitis-related phenotypes in experimental models [19], and barrier-associated processes are mechanistically relevant to neonatal bilirubin physiology because barrier integrity can influence luminal antigen exposure, epithelial transport dynamics, and inflammatory tone—factors that may indirectly shape enterohepatic cycling and bilirubin handling. Tight junction proteins including occludin and ZO-1 are increasingly recognized not only as structural components but also as responsive regulators within epithelial stress and repair programs [41]. The key point for the present manuscript is therefore not that AzA "explains" neonatal HB, but that a measurable, directionally lower candidate signal at birth can be carried forward into an intervention experiment that probes intestinal readouts relevant to the gut–liver axis.

The animal experiment offers a complementary probe, while also requiring careful boundary-setting. In the APH-induced HB model, AzA administration was associated with reduced serum total bilirubin and coincided with increased colonic occludin expression and lower colonic β-glucuronidase activity, alongside a partial shift in fecal microbiome structure toward the control group. These readouts are internally consistent with an intestinally relevant pattern of changes: barrier-related proteins changed in the expected direction, and a microbial functional phenotype (β-glucuronidase activity) moved in parallel with bilirubin reduction. At the same time, the experiment does not, by itself, identify the dominant causal route. AzA could act directly on the host epithelium, indirectly through microbial community changes, or through systemic effects that secondarily influence the gut. Nor do the animal data prove that the meconium AzA difference in humans is causal. The most defensible interpretation is narrower: perturbing AzA levels in a hyperbilirubinemic context is associated with a measurable reduction in bilirubin and with intestinal changes that are mechanistically plausible within a gut–liver framework. Consistent with prior work emphasizing that barrier modulation should not be over-interpreted as direct metabolic causation, we view the occludin signal as supportive of altered epithelial state rather than as proof that AzA targets bilirubin metabolism *per se* [42]. Given the small western blot sample size, ZO-1, included as a complementary marker, is interpreted more cautiously, and we have therefore kept the emphasis on directionally consistent barrier readouts rather than on over-reading any single protein result.

A cautious working hypothesis can nonetheless be articulated by combining the human and animal observations without conflating evidence levels. Clinically, infants who develop HB represent a physiological state in which bilirubin production, conjugation capacity, intestinal transit, feeding dynamics, and enterohepatic cycling are not in balance for their age [1,43]. The neonatal gut environment is rapidly changing, and perturbations—phototherapy among them—can shift microbial succession and metabolic outputs [27,28]. In such a setting, even modest differences in intestinal microbial enzymatic capacity could influence the handling of glucuronidated compounds. A well-established example is bacterial β-glucuronidase activity, which can deconjugate glucuronidated molecules in the gut and thereby influence systemic exposure to reactivated metabolites; this principle is supported in pharmacological contexts [44]. Human neonatal cohort evidence also suggests a dynamic association between bilirubin trajectories and gut microbial genera over the first month of life, consistent with a bidirectional gut–bilirubin relationship rather than a static snapshot [45]. Our human dataset does not measure microbial β-glucuronidase genes or activity, and meconium taxonomic signals remain uncertain in the absence of negative controls; therefore, we avoid proposing a specific "taxon $\rightarrow$ enzyme $\rightarrow$ bilirubin" chain in humans. What the present study suggests is a tractable, testable idea: lower AzA in meconium is a candidate signal associated with HB at the population level, and modulating AzA in an experimental hyperbilirubinemic context moves bilirubin and intestinal readouts in parallel. That is sufficient to justify targeted validation and mechanistic follow-up, but not to justify therapeutic claims.

Several limitations should be addressed proactively, because each can plausibly account for part of the observed signal if left unacknowledged. First, the sample size for multi-omics comparisons is modest, particularly for HB (n = 21), which limits statistical power, increases uncertainty around effect estimates, and reduces the stability of feature selection—especially once FDR correction is applied. This limitation directly explains why the metabolomics findings remain nominal and why we frame AzA as a candidate rather than a validated marker. The mitigation is equally direct: replication in independent datasets with larger HB case numbers, ideally with pre-specified hypotheses and pre-registered analytic plans, is required before any clinical inference is attempted. Second, low-biomass contamination remains a key limitation for genus-level interpretation in meconium (discussed above), and future work should incorporate extraction/PCR blanks, bacterial load quantification, and decontamination workflows [35]. Third, selection and generalizability require careful framing. To reduce heterogeneity in early microbial exposure, our sampling framework focused on a clinically homogeneous birth context (term singleton vaginal deliveries per inclusion criteria). This improves internal consistency for a first-pass meconium question, but it narrows external validity: the results may not generalize to preterm infants, cesarean deliveries, antibiotic-exposed births, or different feeding and care environments. Future studies should treat those groups not as noise but as clinically meaningful strata. Fourth, the human analysis is observational; associations between meconium features and HB cannot establish causality. The animal experiment improves biological plausibility but does not replicate neonatal physiology and therefore cannot be taken as clinical causal proof. Fifth, the APH model reflects hemolysis-driven HB, which differs from common neonatal mechanisms such as developmental immaturity of conjugation pathways; this difference limits clinical translation and reinforces why we avoid any therapeutic language. Finally, mechanistic resolution remains incomplete even within the animal model: we measured serum total bilirubin and intestinal readouts, but we did not partition direct versus indirect bilirubin fractions, nor did we include broader liver injury panels that could help discriminate between production, conjugation, and clearance components; likewise, β-glucuronidase activity was measured at the activity level without distinguishing host versus microbial sources. These gaps define the immediate next experiments rather than undermining the present findings: direct/indirect bilirubin fractionation, liver panel readouts, intestinal transit metrics, and functional microbial assays would substantially sharpen causal inference.

Despite these constraints, the study has two strengths that are directly relevant to early-life microbiome research: it targets a clinically common neonatal condition with an early-life specimen collected at a biologically meaningful time point, and it resists over-interpretation by pairing exploratory human signals with a focused experimental follow-up. The most appropriate reading is therefore modest but actionable. The human meconium analyses nominate candidate microbiome structure differences and a directionally lower AzA signal associated with hyperbilirubinemia at birth, while the animal experiment suggests that AzA perturbation can influence bilirubin and intestinal barrier–related phenotypes in a hyperbilirubinemic setting. The next step is not broader narrative expansion, but rigorous validation and mechanism: replicate AzA directionality and magnitude with targeted quantification in independent neonatal datasets; embed low-biomass controls and absolute bacterial load measures; quantify microbial functional capacity (including β-glucuronidase genes and activity); and test whether the AzA–barrier–bilirubin relationship persists under models that more closely resemble neonatal physiology. Until those steps are completed, AzA should be viewed primarily as a candidate metabolite that justifies mechanistic clarification and carefully designed clinical studies, rather than as a therapeutic agent.

Conclusions

First-pass meconium profiling at birth identified modest community-level microbiome differences between infants with and without HB and highlighted AzA as a directionally lower, hypothesis-generating metabolite signal in HB on nominal testing, without FDR-supported metabolite-level significance. In an APH-induced hyperbilirubinemia rat model, AzA administration was associated with lower serum total bilirubin and coincided with barrier-related intestinal readouts and lower colonic β-glucuronidase activity. These findings are consistent with a gut–liver axis–related hypothesis that can be tested more rigorously in future work, but they do not establish causality or clinical efficacy. Independent replication with low-biomass controls, larger HB sample sizes, and functional assays is required before translational claims are considered.

Abbreviations

16S rRNA, 16S ribosomal RNA; ASV, Amplicon Sequence Variant; AzA, azelaic acid; BMI, Body Mass Index; FDR, False Discovery Rate; HB, Hyperbilirubinemia; HC, Healthy Control; LDA, Linear Discriminant Analysis; PCA, Principal Component Analysis; PCoA, Principal Coordinates Analysis.

Availability of Data and Materials

The dataset will be released upon publication; during peer review, access is available via the BioProject record (accession: PRJNA1405568).

Author Contributions

Conceptualization, LZ and LP; methodology, LZ and QW; software, YZ; validation, ZL, QW and YZ; formal analysis, QW; investigation, ZL; data curation, ZL and YZ; writing—original draft preparation, ZL and XH; writing—review and editing, LZ, LP, QW and YZ; visualization, YZ; supervision, XH; methodology oversight, XH; interpretation of data, XH; project administration, LZ. All authors have read and agreed to the published version of the manuscript. All authors have participated sufficiently in the work to take public responsibility for appropriate portions of the content and agreed to be accountable for all aspects of the work in ensuring that questions related to its accuracy or integrity are appropriately investigated and resolved.

Ethics Approval and Consent to Participate

The cohort was conducted under an ongoing ethics approval granted by the Ethics Committee of the Seventh Medical Center, Chinese PLA General Hospital (Approval No.2021-033). Written informed consent was obtained from parents or legal guardians prior to participation. All procedures were conducted in accordance with the Declaration of Helsinki and relevant regulations. All animal procedures were approved by the Experimental Animal Ethics Committee of Kangtai Medical Laboratory Service Hebei Co., Ltd. (Approval No. MDL2025-06-03-02). The animal study was conducted and reported in accordance with ARRIVE Guideline 2.0.

Acknowledgment

Not applicable.

Funding

This research received no external funding.

Conflict of Interest

The authors declare no conflict of interest.

Supplementary Material

Supplementary material associated with this article can be found, in the online version, at https://doi.org/10.24976/Discov.Med.202638208.116.

References

[1] Kemper AR, Newman TB, Slaughter JL, Maisels MJ, Watchko JF, Downs SM, *et al*. Clinical Practice Guideline Revision: Management of Hyperbilirubinemia in the Newborn Infant 35 or More Weeks of Gestation. Pediatrics. 2022; 150: e2022058859. https://doi.org/10.1542/peds.2022-058859.

[2] Par EJ, Hughes CA, DeRico P. Neonatal Hyperbilirubinemia: Evaluation and Treatment. American Family Physician. 2023; 107: 525–534.

[3] Olusanya BO, Kaplan M, Hansen TWR. Neonatal hyperbilirubinaemia: a global perspective. The Lancet. Child & Adolescent Health. 2018; 2: 610–620. https://doi.org/10.1016/S2352-4642(18)30139-1.

[4] Pillai A, Pandita A, Osiovich H, Manhas D. Pathogenesis and Management of Indirect Hyperbilirubinemia in Preterm Neonates Less Than 35 Weeks: Moving Toward a Standardized Approach. NeoReviews. 2020; 21: e298–e307. https://doi.org/10.1542/neo.21-5-e298.

[5] Hall B, Levy S, Dufault-Thompson K, Arp G, Zhong A, Ndjite GM, *et al*. BilR is a gut microbial enzyme that reduces bilirubin to urobilinogen. Nature Microbiology. 2024; 9: 173–184. https://doi.org/10.1038/s41564-023-01549-x.

[6] Pollet RM, D'Agostino EH, Walton WG, Xu Y, Little MS, Biernat KA, *et al*. An Atlas of β-Glucuronidases in the Human Intestinal Microbiome. Structure (London, England: 1993). 2017; 25: 967–977.e5. https://doi.org/10.1016/j.str.2017.05.003.

[7] Koníčková R, Jirásková A, Zelenka J, Lešetický L, Štícha M, Vítek L. Reduction of bilirubin ditaurate by the intestinal bacterium Clostridium perfringens. Acta Biochimica Polonica. 2012; 59: 289–292. https://doi.org/10.18388/abp.2012_2153.

[8] Dufault-Thompson K, Levy S, Hall B, Jiang X. Bilirubin reductase shows host-specific associations in animal large intestines. The ISME Journal. 2024; 18: wrae242. https://doi.org/10.1093/ismejo/wrae242.

[9] Neurath MF, Artis D, Becker C. The intestinal barrier: a pivotal role in health, inflammation, and cancer. The Lancet. Gastroenterology & Hepatology. 2025; 10: 573–592. https://doi.org/10.1016/S2468-1253(24)00390-X.

[10] Chen Z, Liao S, Wu S, Chen S, Tang Q, Zhou L, *et al*. The Gut–Liver Axis in Liver Disease: Molecular Mechanisms and Therapeutic Targets. MedComm. 2025; 6: e70458. https://doi.org/10.1002/mco2.70458.

[11] Ferretti P, Pasolli E, Tett A, Asnicar F, Gorfer V, Fedi S, *et al*. Mother-to-Infant Microbial Transmission from Different Body Sites Shapes the Developing Infant Gut Microbiome. Cell Host & Microbe. 2018; 24: 133–145.e5. https://doi.org/10.1016/j.chom.2018.06.005.

[12] Wilson BC, Butler ÉM, Grigg CP, Derraik JGB, Chiavaroli V, Walker N, *et al*. Oral administration of maternal vaginal microbes at birth to restore gut microbiome development in infants born by caesarean section: A pilot randomised placebo-controlled trial. EBioMedicine. 2021; 69: 103443. https://doi.org/10.1016/j.ebiom.2021.103443.

[13] Chang YS, Li CW, Chen L, Wang XA, Lee MS, Chao YH. Early Gut Microbiota Profile in Healthy Neonates: Microbiome Analysis of the First-Pass Meconium Using Next-Generation Sequencing Technology. Children (Basel, Switzerland). 2023; 10: 1260. https://doi.org/10.3390/children10071260.

[14] Kielenniva K, Ainonen S, Vänni P, Paalanne N, Renko M, Salo J, *et al*. Microbiota of the first-pass meconium and subsequent atopic and allergic disorders in children. Clinical and Experimental Allergy: Journal of the British Society for Allergy and Clinical Immunology. 2022; 52: 684–696. https://doi.org/10.1111/cea.14117.

[15] Nunez H, Nieto PA, Mars RA, Ghavami M, Sew Hoy C, Sukhum K. Early life gut microbiome and its impact on childhood health and chronic conditions. Gut Microbes. 2025; 17: 2463567. https://doi.org/10.1080/19490976.2025.2463567.

[16] Ding J, Ma X, Han L, Zhao X, Li A, Xin Q, *et al*. Gut microbial alterations in neonatal jaundice pre- and post-treatment. Bioscience Reports. 2021; 41: BSR20210362. https://doi.org/10.1042/BSR20210362.

[17] Yu Q, Lu T, Yan J, Shen N, Wu R, Liu S, *et al*. Changes in the Gut Microbiota of Neonates with Hyperbilirubinemia Reaching Phototherapy Thresholds. International Journal of General

Medicine. 2025; 18: 5001–5011. https://doi.org/10.2147/IJGM.S531481.

[18] Chen W, Zhang P, Zhang X, Xiao T, Zeng J, Guo K, *et al*. Machine learning-causal inference based on multi-omics data reveals the association of altered gut bacteria and bile acid metabolism with neonatal jaundice. Gut Microbes. 2024; 16: 2388805. https://doi.org/10.1080/19490976.2024.2388805.

[19] Liao Y, Wu X, Luo W, Chen J, Huang Y, Ma K, *et al*. Azelaic Acid Regulates the Renin-Angiotensin System and Improves Colitis Based on Network Pharmacology and Experimentation. ACS Omega. 2023; 8: 15217–15228. https://doi.org/10.1021/acsomega.3c00210.

[20] Feng X, Shang J, Gu Z, Gong J, Chen Y, Liu Y. Azelaic Acid: Mechanisms of Action and Clinical Applications. Clinical, Cosmetic and Investigational Dermatology. 2024; 17: 2359–2371. https://doi.org/10.2147/CCID.S485237.

[21] Percie du Sert N, Hurst V, Ahluwalia A, Alam S, Avey MT, Baker M, *et al*. The ARRIVE guidelines 2.0: Updated guidelines for reporting animal research. PLoS Biology. 2020; 18: e3000410. https://doi.org/10.1371/journal.pbio.3000410.

[22] Chinese Society of Pediatrics, Neonatology Group; Editorial Board of Chinese Journal of Pediatrics. Expert consensus on the diagnosis and treatment of neonatal hyperbilirubinemia. Chinese Journal of Pediatrics. 2014; 52: 745–748. https://doi.org/10.3760/cma.j.issn.0578-1310.2014.10.006. (In Chinese)

[23] Qattea I, Farghaly MAA, Elgendy M, Mohamed MA, Aly H. Neonatal hyperbilirubinemia and bilirubin neurotoxicity in hospitalized neonates: analysis of the US Database. Pediatric Research. 2022; 91: 1662–1668. https://doi.org/10.1038/s41390-021-01692-3.

[24] Merino-Andrés J, Pérez-Nombela S, Álvarez-Bueno C, Hidalgo-Robles Á, Ruiz-Becerro I, Fernández-Rego FJ. Neonatal hyperbilirubinemia and repercussions on neurodevelopment: A systematic review. Child: Care, Health and Development. 2024; 50: e13183. https://doi.org/10.1111/cch.13183.

[25] Lin C, Lin Y, Xiao R, Guo M, Zhang H, Chen W, *et al*. Bifidobacterium species associated with breastfeeding alleviate neonatal hyperbilirubinaemia via the gut microbiota-α-linolenic and linoleic acid metabolism-enterohepatic circulation axis. Microbiome. 2025; 13: 187. https://doi.org/10.1186/s40168-025-02190-y.

[26] Lin T, Chen Y, Liu L, Wu T, Qian Y, Jin B. Recent advances in gut microbiota metabolite regulation of hepatic pregnane X receptor. Frontiers in Immunology. 2025; 16: 1692684. https://doi.org/10.3389/fimmu.2025.1692684.

[27] Zhang K, Fan S, Lv A, Ma Y, Fang X, Zhang J. Integrated analysis of microbiota with bile acids for the phototherapy treatment of neonatal jaundice. Archives of Medical Science: AMS. 2021; 19: 401–410. https://doi.org/10.5114/aoms/134023.

[28] Wu R, Jiang Y, Yan J, Shen N, Liu S, Yin H, *et al*. Beneficial changes in gut microbiota after phototherapy for neonatal hyperbilirubinemia. Biomedical Reports. 2024; 20: 101. https://doi.org/10.3892/br.2024.1789.

[29] Chen K, Yuan T. The role of microbiota in neonatal hyperbilirubinemia. American Journal of Translational Research. 2020; 12: 7459–7474.

[30] Turunen J, Tejesvi MV, Paalanne N, Pokka T, Amatya SB, Mishra S, *et al*. Investigating prenatal and perinatal factors on meconium microbiota: a systematic review and cohort study. Pediatric Research. 2024; 95: 135–145. https://doi.org/10.1038/s41390-023-02783-z.

[31] Dos Santos SJ, Pakzad Z, Elwood CN, Albert AYK, Gantt S, Manges AR, *et al*. Early Neonatal Meconium Does Not Have a Demonstrable Microbiota Determined through Use of Robust Negative Controls with *cpn*60-Based Microbiome Profiling. Microbiology Spectrum. 2021; 9: e0006721. https://doi.org/10.1128/Spectrum.00067-21.

[32] Fierer N, Leung PM, Lappan R, Eisenhofer R, Ricci F, Holland SI, *et al*. Guidelines for preventing and reporting contamination in low-biomass microbiome studies. Nature Microbiology. 2025; 10: 1570–1580. https://doi.org/10.1038/s41564-025-02035-2.

[33] Dyrhovden R, Rippin M, Øvrebø KK, Nygaard RM, Ulvestad E, Kommedal Ø. Managing Contamination and Diverse Bacterial Loads in 16S rRNA Deep Sequencing of Clinical Samples: Implications of the Law of Small Numbers. mBio. 2021; 12: e0059821. https://doi.org/10.1128/mBio.00598-21.

[34] Austin GI, Korem T. Planning and Analyzing a Low-Biomass Microbiome Study: A Data Analysis Perspective. The Journal of Infectious Diseases. 2026; 233: 76–86. https://doi.org/10.1093/infdis/jiae378.

[35] Dean CJ, Deng Y, Wehri TC, Pena-Mosca F, Ray T, Crooker BA, *et al*. The impact of kit, environment, and sampling contamination on the observed microbiome of bovine milk. mSystems. 2024; 9: e0115823. https://doi.org/10.1128/msystems.01158-23.

[36] Yang L, Chen J. A comprehensive evaluation of microbial differential abundance analysis methods: current status and potential solutions. Microbiome. 2022; 10: 130. https://doi.org/10.1186/s40168-022-01320-0.

[37] Nearing JT, Douglas GM, Hayes MG, MacDonald J, Desai DK, Allward N, *et al*. Microbiome differential abundance methods produce different results across 38 datasets. Nature Communications. 2022; 13: 342. https://doi.org/10.1038/s41467-022-28034-z.

[38] Lin H, Peddada SD. Multigroup analysis of compositions of microbiomes with covariate adjustments and repeated measures. Nature Methods. 2024; 21: 83–91. https://doi.org/10.1038/s41592-023-02092-7.

[39] Alseekh S, Aharoni A, Brotman Y, Contrepois K, D'Auria J, Ewald J, *et al*. Mass spectrometry-based metabolomics: a guide for annotation, quantification and best reporting practices. Nature Methods. 2021; 18: 747–756. https://doi.org/10.1038/s41592-021-01197-1.

[40] Beger RD, Goodacre R, Jones CM, Lippa KA, Mayboroda OA, O'Neill D, *et al*. Analysis types and quantification methods applied in UHPLC-MS metabolomics research: a tutorial. Metabolomics: Official Journal of the Metabolomic Society. 2024; 20: 95. https://doi.org/10.1007/s11306-024-02155-6.

[41] Kuo WT, Odenwald MA, Turner JR, Zuo L. Tight junction proteins occludin and ZO-1 as regulators of epithelial proliferation and survival. Annals of the New York Academy of Sciences. 2022; 1514: 21–33. https://doi.org/10.1111/nyas.14798.

[42] Nie HY, Ge J, Huang GX, Liu KG, Yue Y, Li H, *et al*. New insights into the intestinal barrier through "gut-organ" axes and a glimpse of the microgravity's effects on intestinal barrier. Frontiers in Physiology. 2024; 15: 1465649. https://doi.org/10.3389/fphys.2024.1465649.

[43] Su H, Yang S, Chen S, Chen X, Guo M, Zhu L, *et al*. What Happens in the Gut during the Formation of Neonatal Jaundice-Underhand Manipulation of Gut Microbiota? International Journal of Molecular Sciences. 2024; 25: 8582. https://doi.org/10.3390/ijms25168582.

[44] Gao S, Sun R, Singh R, Yu So S, Chan CTY, Savidge T, *et al*. The role of gut microbial β-glucuronidase in drug disposition and development. Drug Discovery Today. 2022; 27: 103316. https://doi.org/10.1016/j.drudis.2022.07.001.

[45] Li Z, Zhang Y, Luo X, Wang Y, Peng L, Zou L. Dynamic relationships between bilirubin concentrations and the gut microbiota in the neonatal period: A pilot prospective cohort study. Pediatric Investigation. 2025; 9: 347–360. https://doi.org/10.1002/ped4.70032.